Robot-based measurement system for double-sided inspection of optical components

Daniel Wertjanz, Thomas Kern, Ernst Csencsics and Georg Schitter, *Senior Member, IEEE*
Group for Advanced Mechatronic Systems
Automation and Control Institute (ACIN), TU Wien
1040 Vienna, Austria
wertjanz@acin.tuwien.ac.at

***Abstract*—This paper presents a robotic measurement system for the precise double-sided inline inspection of optical elements. The robotic system includes an electromagnetically actuated measurement platform (MP), capable of inducing a stiff link between the integrated high precision confocal chromatic sensor (CCS) and the sample by means of feedback control. In this way, disturbing relative motion between the CCS and the sample are compensated, establishing the desired lab-like conditions during the point-wise acquired 3D measurement. The high-precision positioning capability of the MP is used to precisely move the CCS' measurement spot across the sample surface in a tailored scan pattern. The robotic 3D measurement system provides a lateral measurement area of $4 \times 4\,\mathrm{mm}^2$ and achieves a lateral and axial resolution of $5\,\mu\mathrm{m}$ and $130\,\mathrm{nm}$, respectively. In addition, high-precision 3D measurements of arbitrary regions of interest can be performed. Experimental results of a commercial lenslet array demonstrate, that the robotic sample-tracking system increases the double-sided surface and thickness measurement performance by at least one order of magnitude compared to the state-of-the-art approach, while enabling the detection of surface defects on the sub-micrometer scale.**

***Index Terms*—Mechatronics, optoelectronic sensors, robotic 3D measurement systems**

I. Introduction

High-precision manufacturing of optical elements is a key factor of modern industrial production [1]. Due to the ongoing trend of miniaturizing opto-electronic devices, free-formed optical elements with complex geometry and shape are highly demanded [2]. The fields of application range from micro-lens arrays for enhanced light absorption in solar cells [3] to contact lens displays for augmented reality [4] and freeform lenses for uniform light illumination [5].

In order to measure the surface shape and quality of optical elements, precise and flexible measurement systems are required [6]. Especially for industrially mass-produced goods, such as injection-molded optical elements [7], inline measurement systems for free-formed optics are of growing interest. Industrial robots (IRs) are an appropriate tool to enable the desired measurement flexibility [8]. Besides a continuous and 100 % quality monitoring, robotic inline measurement systems can enable realtime optimization of production parameter settings to significantly increase the product reliability and the production yield [9], [10]. However, the positioning uncertainty of modern IRs is in the range of several tens of micrometers, which makes robots directly equipped with 3D measurement tools not suitable for high-precision inline measurements on the single or even sub-micrometer scale [11].

Coordinate measurement machines (CMMs) are typically deployed to perform high-precision surface measurements of optical elements, which incorporate a multi-degree of freedom (DoF) positioning system for a 1-D sensor [12]. In order to avoid the unfavorable need of flipping the sample between two sequentially acquired top and bottom surface measurements, confocal chromatic sensors (CCSs) can be used to enable the targeted double-sided measurements of optical elements [13]. CMMs are usually operated in a vibration-free lab environment, which is, however, in complete contrary to the vibration-prone environment of an industrial production line. Similar to the limited positioning precision of IRs, environmental disturbances can cause relative motion between the measurement tool and the sample, resulting in 3D measurements corrupted by motion blur [14]. This task is further aggravated when targeting thickness measurements of optical elements, such as micro-lenses. High-precision 3D measurements are therefore usually performed in a vibration-free lab environment, spatially separated from the production line. Consequently, a 100% quality control of mass-produced optical elements is typically infeasible without impairing the production yield.

In order to enable reliable and efficient high-precision inline measurements, a robotic 3D measurement system has been developed recently [15]. With an electromagnetically levitated measurement platform (MP) actively tracking the sample surface in six DoFs, disturbance-induced relative motion between measurement tool (MT) and sample is compensated and local lab-like conditions are established during the high-precision measurement. The robotic system incorporates a high-precision 3D MT, which is currently limited to single-sided 3D measurements of structural surfaces.

This project is partially funded by the Hochschuljubiläumsfonds of the city of Vienna, Austria under the project number H-260744/2020. The financial support by the Austrian Federal Ministry for Digital and Economic Affairs, and the National Foundation for Research, Technology and Development, as well as MICRO-EPSILON MESSTECHNIK GmbH & Co. KG and ATENSOR Engineering and Technology Systems GmbH is gratefully acknowledged.

Post-print version of the article: D. Wertjanz, T. Kern, E. Csencsics, and G. Schitter, "Robot-based measurement system for double-sided inspection of optical components," *2023 IEEE International Instrumentation and Measurement Technology Conference (I2MTC)*, Kuala Lumpur, Malaysia, 2023. DOI: 10.1109/I2MTC53148.2023.10175937

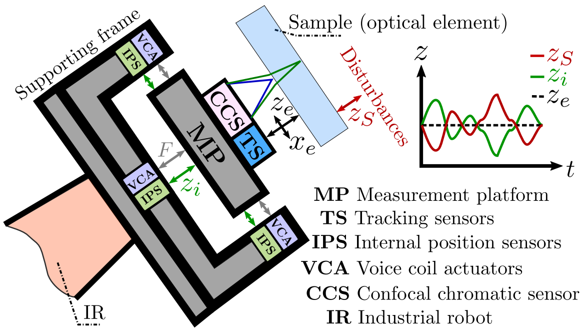

Fig. 1: Robotic inline system for double-sided surface measurements of transparent optical elements. A CCS is mounted to a sample-tracking MP. Disturbance-induced relative motion z_S is actively compensated by maintaining a constant position z_e between CCS and sample.

The contribution of this paper is the integration of a robotic inline measurement system for the double-sided high-precision surface inspection of optical components.

The combination of the double-sided measurement capability of a CCS with the high-precision positioning of the MP appears as a viable approach to precisely scan the CCS' measurement spot across the sample, avoiding a disturbance-induced misalignment of the light beam.

II. Robotic double-sided surface measurement system

The concept of the robotic inline system for high-precision double-sided surface measurements is schematically illustrated in Fig. 1. Acting as end-effector of an IR, an electromagnetically levitated MP carries a high-precision CCS, which is capable of point-wise measuring the top- and bottom-side of a thin optical element. Integrated high-precision tracking sensors (TSs) are measuring the CCS' out-of-plane and in-plane position z_e and x_e relative to the sample surface. By means of feedback control, the out-of-plane position z_e is maintained constant, introducing a contactless stiff link between CCS and sample by compensating disturbance- as well as robot-induced relative motion in z_S.

With the MP actively tracking the sample, local lab-like conditions are established for the CCS. Superimposed to the compensation of the disturbance-induced relative motion, the MP's precise positioning capability is used to scan the CCS's measurement spot across the sample. With the MP acting as fine actuator, the internal position sensor (IPS) system is used as feedback signal to reposition the IR (coarse actuator) such that the free-floating MP stays in its actuation range.

III. System design and prototype

Considering the system concept in Fig. 1, the cross-section of the CAD model and the implemented prototype of the robotic measurement system are shown in Fig. 2. Being the system's core components, the sample-tracking MP and the CCS are discussed in the following.

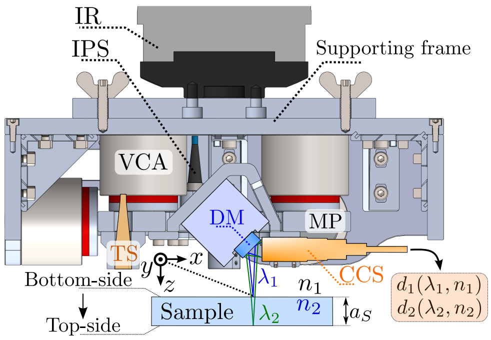

(a) CAD model.

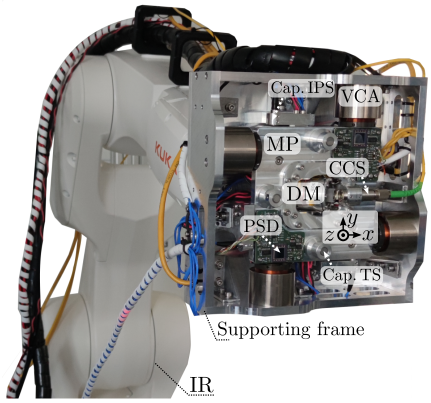

(b) System prototype.

Fig. 2: System design and implemented prototype. The VCA-actuated sample-tracking MP carries a high-precision CCS. Via a DM, the CCS' light beam is aligned to the transparent sample. Integrated IPSs and TSs measure the internal and external MP position in six DoFs.

A. Sample-tracking measurement platform

With the MP being actuated within the air gaps of eight identical voice coil actuators (VCAs), an actuation range of about 300 µm is achieved in the translational DoFs [14]. Three capacitive TSs measure the MP's out-of-plane position relative to the sample. A position-sensitive device (PSD)-based sensor system is integrated in order to measure the according in-plane position, which uses laser-based markers mounted on a custom-made sample box. In all six DoFs, the integrated controller is designed for a sample-tracking bandwidth of 450 Hz [15], ensuring a precise alignment of the CCS relative to the sample. In the translational in- and out-of-plane DoFs, a static positioning uncertainty of about 220 nm @ 1σ and 30 nm @ 1σ is achieved.

Additional six capacitive IPSs measure the MP's position relative to the supporting frame (internal position), i.e. relative to the IR. Using this measured position, an internal position

Post-print version of the article: D. Wertjanz, T. Kern, E. Csencsics, and G. Schitter, "Robot-based measurement system for double-sided inspection of optical components," *2023 IEEE International Instrumentation and Measurement Technology Conference (I2MTC)*, Kuala Lumpur, Malaysia, 2023. DOI: 10.1109/I2MTC53148.2023.10175937

controller is integrated to stabilize the MP in its free-floating center position when the TSs are out-of-range.

B. Confocal chromatic sensor

Using longitudinal chromatic aberration for distance and thickness measurements, a CCS achieves an axial resolution in the nanometer range [16]. Therefore, the compact CCS head IFS2404-2 (Micro-Epsilon, Ortenburg, Germany) is selected to enable the point-wise acquired double-sided measurement of optical elements. The selected CCS provides an axial resolution of up to 40 nm, a spot diameter of 10 µm and a maximum measurement rate of 70 kHz. An adjustable deflection mirror (DM) is integrated to ensure a good alignment of the CCS' light beam on the sample.

Considering the double-sided measurement in Fig. 2a, the two confocal chromatic components reflected at the sample's bottom- and top-side are redirected to a spectrometer through a pinhole, with the according wavelengths λ_1 and λ_2 being identified via a peak detection in the intensity profile. Using the known refraction index of the transmission medium, in this case air ($n_1 \approx 1$), as well as of the sample n_2, the sample thickness is given by

$$a_S(\lambda_1, \lambda_2, n_1, n_2) = d_2(\lambda_2, n_1, n_2) - d_1(\lambda_1, n_1), \qquad (1)$$

with $d_1(\lambda_1, n_1)$ and $d_2(\lambda_2, n_1, n_2)$ the distances between CCS and bottom side, and between CCS and top side. Considering air as transmission medium, the spectral components of the CCS' white light source are focused at distances between 14 and 16 mm along its optical axis. Consequently, the maximum measurable thickness (see Fig. 2a) of the transparent sample under test is given by

$$a_{\text{S,max}} = m_r \cdot n_2, \qquad (2)$$

with $m_r = 2\,\text{mm}$ being the measurement range of the selected CCS in air.

IV. Double-sided measurement setup

A. Measurement routine

In Fig. 3, the block diagram of the integrated robotic sample-tracking system for double-sided surface inspection is shown. The lateral scan trajectory (x_{ref}, y_{ref}) is calculated by a trajectory generator and applied to the MP's reference position $\zeta_{e,r}$ of the sample-tracking control. In order to ensure a constant alignment of the CCS relative to the sample, the reference position in the remaining DoFs is maintained constant. For each discrete time step, the measured translational in-plane position x, y of the MP together with the according distances d_1 and d_2 measured by the CCS are stored. Subsequently, the acquired signals are applied to an image processing procedure, in which invalid data points are removed, the remaining measurement data is fitted into an equidistant grid and smoothing filters are applied. In this way, both measured distances are mapped into the xy-grid and two individual 3D surface measurements for the sample's bottom- and top-side are obtained. Additionally, the 3D data of the sample thickness can be calculated using the relation in (1).

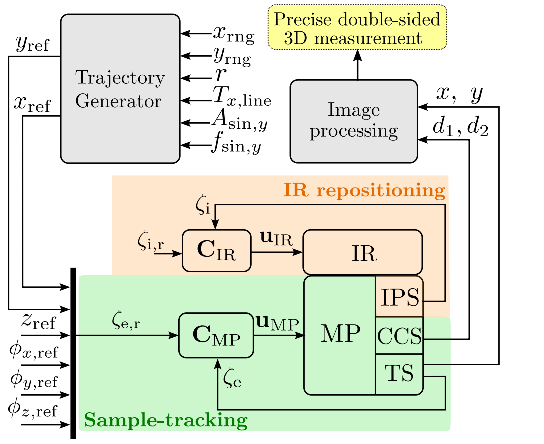

Fig. 3: Block diagram of the measurement setup enabling precise robotic double-sided 3D surface measurements.

To extend the MP's limited translational actuation range of 300 µm, a dual stage control approach is implemented [17]. Therefore, a parent-child configuration is implemented, in which the IR (child) is repositioned, such that the MP (parent) is maintained within its actuation range. Based on the difference between the measured MP's internal position ζ_i and its center position $\zeta_{i,r}$, the output $\mathbf{u}_{\text{IR}}$ calculated by the controller $\mathbf{C}_{\text{IR}}$ is applied to the IR. The implemented dual stage approach extends the MP actuation range to 4 mm in x- and y-direction, limited by the PSD-based in-plane sensor system [15]. The IR position control bandwidth of 0.5 Hz enables a high-precision full-range in-plane motion of 4 mm within a minimum time of 5 s.

B. Measurement trajectory design

Considering the CCS' measurement spot diameter of 10 µm and the dual stage-controlled MP's lateral range of 4 mm, a full-frame and dense 3D measurement would require $\frac{4\,\text{mm}}{10\,\mu\text{m}}$ lines $\cdot$ 5 s/line = 33 min. Considering the system's targeted inline application, a time-efficient measurement trajectory is required. Being a suitable trade-off between a smooth scan trajectory to avoid high accelerations and a dense scan pattern performed within a reasonable measurement time, a raster scan with a super-imposed sine motion in y-direction is proposed and shown in Fig. 4 (red). Depending on the specific sample under test, the MP's scan trajectory (x_{ref}, y_{ref}) can be adjusted by several measurement parameters, which are applied to the trajectory generator (see Fig. 3). In this relation, x_{rng} and y_{rng} denote the desired lateral measurement range, r the line distance, $T_{\text{x,line}}$ the measurement time for a single line scan in x-direction as well as $A_{\text{sin,y}}$ and $f_{\text{sin,y}}$ the amplitude and frequency of the superimposed sine motion applied in y-direction. As can be seen in Fig. 4, the superimposed sine motion applied to the MP in y-direction (red) significantly increases the scan pattern density for a certain line distance r compared to a conventional raster scan (black). Although

Post-print version of the article: D. Wertjanz, T. Kern, E. Csencsics, and G. Schitter, "Robot-based measurement system for double-sided inspection of optical components," *2023 IEEE International Instrumentation and Measurement Technology Conference (I2MTC)*, Kuala Lumpur, Malaysia, 2023. DOI: 10.1109/I2MTC53148.2023.10175937

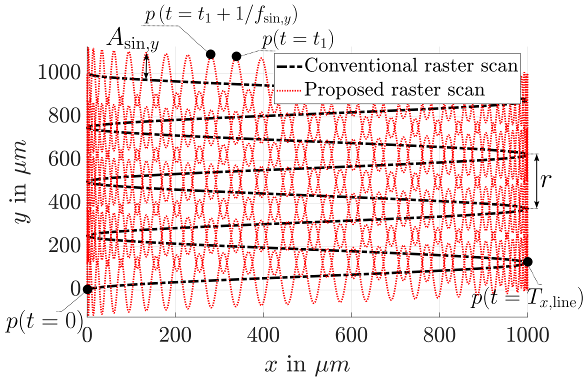

Fig. 4: Scan trajectory ($x_{\text{rng}} = y_{\text{rng}} = 1\,\text{mm}$, $r = 250\,\mu\text{m}$, $T_{\text{x,line}} = 5\,\text{s}$, $A_{\text{sin,y}} = 125\,\mu\text{m}$, $f_{\text{sin,y}} = 5\,\text{Hz}$). The superimposed and higher-frequent sine motion on the y-axis significantly increases the scan pattern density for a certain line distance r.

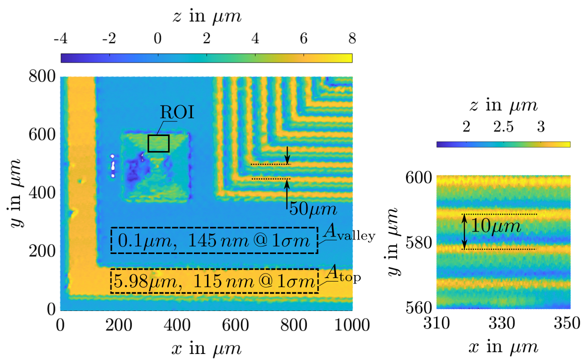

(a) Single-sided overview scan. (b) RoI scan.

Fig. 5: Single-sided 3D measurement for evaluating the system's lateral and axial resolution. a) shows an overview scan of the sample's structural surface. In b), the 3D measurement result of the RoI indicated in a) is shown.

the IR position control bandwidth is limited to $0.5\,\text{Hz}$, the superimposed sine frequency $f_{\text{sin,y}}$ and the corresponding amplitude $A_{\text{sin,y}}$ can be set up to several tens of Hertz and $100\,\mu\text{m}$, respectively. In this configuration, the MP stays within its actuation range and does not require the IR to follow the faster superimposed scanning motion. For the exemplarily shown trajectory, the pattern density is increased by about factor 12.5, which corresponds to the increase of the travelled MP distance.

V. Experimental performance evaluation

With the active sample-tracking robotic measurement system operational, the achieved lateral and axial resolution is determined in a first step. Based on these results, the double-sided and thickness measurement performance is demonstrated on an optical freeform surface.

A. 3D measurement resolution and uncertainty

A step-height-standard (Nanuler Calibration Standard, Applied NanoStructures Inc., Mountain view, CA, USA) with a structural height of $5.81\,\mu\text{m}$ is used to evaluate the lateral and axial resolution of the robotic 3D measurement system in a single-sided measurement configuration. Therefore, the calibration standard is placed on the custom sample holder and the robotic system is aligned to it [15]. Considering the scan pattern discussed in Section IV, the parameters $x_{\text{rng}} = 1\,\text{mm}$, $y_{\text{rng}} = 0.8\,\text{mm}$, $r = 20\,\mu\text{m}$, $T_{\text{x,line}} = 10\,\text{s}$, $A_{\text{sin,y}} = 10\,\mu\text{m}$, $f_{\text{sin,y}} = 10\,\text{Hz}$ are set, and the generated trajectory is applied to the MP. These parameters correspond to a total measurement time of $T_m = 800\,\text{s}$.

The obtained single-sided 3D measurement is shown in Fig. 5a. A plane is fitted into the 3D data and subtracted from the 3D point cloud. As can be seen on the top-right, a part of the step-height-standard's magnification boxes are visible, with the pitch of $50\,\mu\text{m}$ in x- and y-direction correctly measured. By evaluating the structural height in the surface area of A_{valley}, a mean height of $0.1\,\mu\text{m}$ with an uncertainty of $145\,\text{nm}\,@\,1\sigma$ is obtained. For the scan area A_{top} on the structural step in Fig. 5a (bottom), a height of $5.98\,\mu\text{m}$ with an uncertainty of $115\,\text{nm}\,@\,1\sigma$ is measured. Comparing the measured mean structural height of with the defined structural height of $5.81\,\mu\text{m}$, an accuracy of about 99% is achieved. In this relation, the mean uncertainty of $130\,\text{nm}\,@\,1\sigma$ is considered as the axial resolution.

Looking at the top-left in Fig. 5a, the $10\,\mu\text{m}$ pitch grating in the region of interest (RoI) is not visible for the applied measurement parameters. Therefore, a detailed RoI scan ($x_{\text{rng}} = y_{\text{rng}} = 40\,\mu\text{m}$, $r = 20\,\mu\text{m}$, $T_{\text{x,line}} = 10\,\text{s}$, $A_{\text{sin,y}} = 10\,\mu\text{m}$, $f_{\text{sin,y}} = 1\,\text{Hz}$) within a measurement time of $T_m = 80\,\text{s}$ is performed. Using this measurement configuration, the $10\,\mu\text{m}$ pitch of the grating structure becomes clearly visible. It is notable, that the structural height is not measured correctly due to the CCS' spot diameter of $10\,\mu\text{m}$ being twice the width of the grating valley. Nonetheless, top and valley of the grating structure can be clearly distinguished, which is why a lateral resolution of better than $5\,\mu\text{m}$ is stated.

B. Double-sided robotic 3D measurements

In order to demonstrate the double-sided surface and thickness measurement capability of the robotic measurement system, a PMMA lenslet array (MLA1, Thorlabs Inc., United States) with a nominal thickness of $1.2 \pm 0.1\,\text{mm}$ and a refractive index of $n_2 = 1.4906$ is used. The lenslet array is placed on the sample box and measured from the backside, i.e. the flat surface is the bottom-side (see Fig. 2a). To evaluate the performance of the developed system, a benchmark measurement is required. Therefore, the MP is stabilized with respect to the IR, resembling an IR directly equipped with a CCS and without sample-tracking capability, which is considered as the state-of-the-art approach.

Post-print version of the article: D. Wertjanz, T. Kern, E. Csencsics, and G. Schitter, "Robot-based measurement system for double-sided inspection of optical components," *2023 IEEE International Instrumentation and Measurement Technology Conference (I2MTC)*, Kuala Lumpur, Malaysia, 2023. DOI: 10.1109/I2MTC53148.2023.10175937

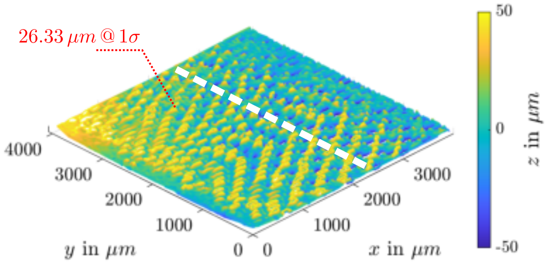

(a) Bottom-side (benchmark).

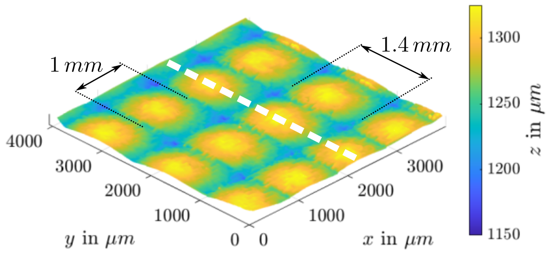

(b) Thickness (benchmark).

Fig. 6: Benchmark measurement of the lenslet array with the CCS rigidly connected to the IR and without sample-tracking. Motion blur corrupts the 3D surface measurement of the flat bottom-side in a). A structural height uncertainty of 26.33 µm @ 1σ is measured. In b), the measured sample thickness reveals the structure of the lenslet array.

Applying the generated scan trajectory for the parameters $x_{\text{rng}} = y_{\text{rng}} = 4\,\text{mm}$, $r = 100\,\mu\text{m}$, $T_{\text{x,line}} = 5\,\text{s}$, $A_{\text{sin,y}} = 50\,\mu\text{m}$, $f_{\text{sin,y}} = 10\,\text{Hz}$ with a total measurement time of $T_m = 400\,\text{s}$ to the IR, the measured bottom-side and thickness of the sample are shown in Fig. 6. As can be seen in the 3D measurement of the flat bottom-side (Fig. 6a), motion blur corrupts the 3D measurements, which is caused by the limited positioning precision of the IR. The measured uncertainty of 26.33 µm @ 1σ in the structural height is in the order of a typical IR's positioning precision of several tens of micrometers [11]. Consequently, the state-of-the-art approach is not expedient to detect surface defects on the single- nor on the sub-micrometer scale.

As the relation for measuring the sample's thickness in (1) is a relative one per definition, the lenslet array's structure becomes visible in the corresponding thickness measurement in Fig. 6b. Although the sample's structural pitch of 1 mm in x- and 1.4 mm in y-direction is measured correctly, the entire 3D measurement of the sample's thickness appears rather blurry.

Repeating the measurement with the active sample-tracking approach, the 3D measurement of the bottom-side and the sample thickness are shown in Fig. 7. In the 3D measurement of the bottom-side (see Fig. 7a), a structural height uncertainty of 554 nm @ 1σ is measured. As indicated in dotted white, structural indentations with a depth of about 1 µm are measured on the same lateral positions as the individual lenses are located in Fig. 7b. These measured surface defects may be caused by the curing process of the injection-molded manufacturing process. Compared to the benchmark measurement of the sample's thickness in Fig. 6b, the thickness measurement obtained by the sample-tracking approach in Fig. 7b appears less blurry.

In order to quantify the system's measurement performance compared to the benchmark approach, the cross-sections at $x = 2325\,\mu\text{m}$ of both double-sided measurements, indicated by the dashed white line in Fig. 6 and 7, are evaluated and shown in Fig. 8. The cross-sectional measurement can be efficiently performed within a measurement time of 5 s. A maximum sample thickness of 1.28 mm is measured by both approaches, which is well within the nominal thickness of 1.2 ± 0.1 mm stated in the lenslet array's data sheet. Evaluating the structural height of the flat bottom-side, the sample-tracking robotic system reduces the surface measurement uncertainty from 24.03 µm @ 1σ to 559 nm @ 1σ, equalling a performance increase by more than factor 40. A lens segment height of 57 µm and 88 µm is measured with the benchmark and the sample-tracking approach, respectively. Considering the lens segment's nominal height of 92 µm to be true, the sample-tracking system reduces the double-sided measurement error by about factor 10.

In summary, the developed robotic sample-tracking system improves the double-sided and thickness measurement performance of optical elements by at least one order of magnitude compared to the state-of-the-art approach and achieves an axial resolution of 130 nm.

VI. Conclusion

In this paper, a robotic measurement system for the precise double-sided inspection of optical elements is developed. By means of a feedback control-induced contactless stiff link, disturbing relative motion between the CCS and the sample are compensated, establishing lab-like conditions during the point-wise acquisition of the double-sided 3D measurement. The high-precision positioning capability of the MP enables the precise scanning of the CCS' measurement spot across the sample, avoiding a disturbance-induced misalignment of the light beam. The robotic 3D measurement system achieves a lateral measurement area of $4 \times 4\,\text{mm}^2$ with a lateral and axial resolution of 5 µm and 130 nm, respectively. Moreover, high-precision RoI scans can be performed at arbitrary locations. The system's double-sided 3D measurement performance is experimentally evaluated on a commercial lenslet array. Compared to the robotic state-of-the-art approach, the sample-tracking system increases the double-sided surface and thickness measurement performance for the transparent optical elements by at least one order of magnitude and enables the detection of surface defects on the sub-micrometer scale.

Post-print version of the article: D. Wertjanz, T. Kern, E. Csencsics, and G. Schitter, "Robot-based measurement system for double-sided inspection of optical components," *2023 IEEE International Instrumentation and Measurement Technology Conference (I2MTC)*, Kuala Lumpur, Malaysia, 2023. DOI: 10.1109/I2MTC53148.2023.10175937

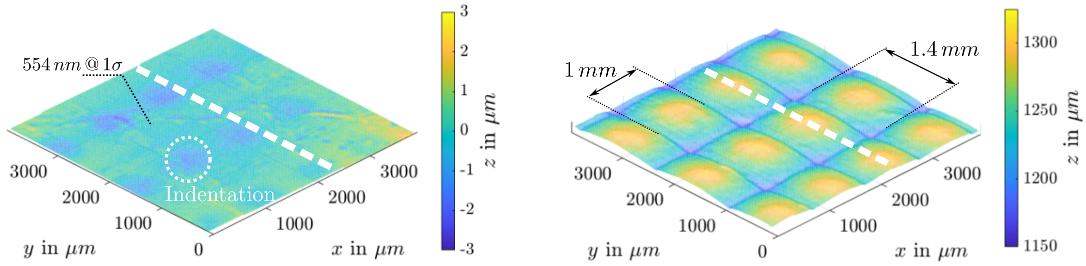

(a) Bottom-side. (b) Thickness.

Fig. 7: Robotic high-precision double-sided inspection of the lenslet array. The structural height uncertainty of the sample's flat bottom-side is evaluated to 554 nm @ 1σ in a). In b), the corresponding sample thickness indicates the lenslet array's structure with the pitch of 1 mm in x- and 1.4 mm in y-direction correctly measured.

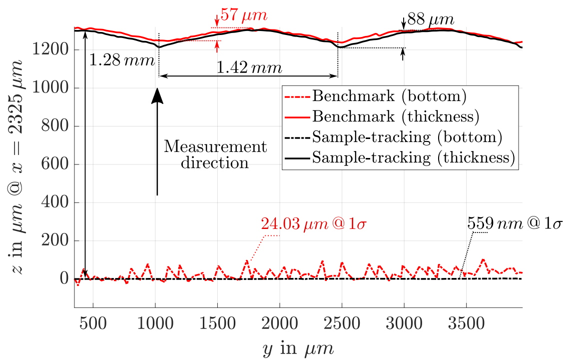

Fig. 8: Cross-section analysis of the double-sided measurements in Fig. 6 and 7 at $x = 2325\,\mu\text{m}$. The sample-tracking system reduces the structural height uncertainty of the flat bottom-side from 24.03 µm @ 1σ (dashed-dotted red) to 559 nm @ 1σ (dashed-dotted black). A pitch of 1.42 mm and maximum sample thickness of 1.28 mm are measured in both approaches. A segment height of 57 µm and 88 µm is measured with the benchmark and the sample-tracking approach, respectively.

Future work includes the robotic double-sided surface and thickness measurements of industrially produced optical elements on a moving conveyor belt.

References

[1] L. Zhu, Z. Li, F. Fang, H. Siyu, and X. Zhang, "Review on fast tool servo machining of optical freeform surfaces," *The International Journal of Advanced Manufacturing Technology*, vol. 95, p. 2071–2092, 03 2018.

[2] J.-M. Lee, D. Lee, and Y. Baek, "Fabrication of dual-focus dual-layered microlens," *Optics Communications*, vol. 289, pp. 69–74, 2013.

[3] A. Peer, R. Biswas, J.-M. Park, R. Shinar, and J. Shinar, "Light management in perovskite solar cells and organic leds with microlens arrays," *Optics express*, vol. 25, no. 9, pp. 10 704–10 709, 2017.

[4] J. Chen, L. Mi, C. P. Chen, H. Liu, J. Jiang, and W. Zhang, "Design of foveated contact lens display for augmented reality," *Optics Express*, vol. 27, no. 26, pp. 38 204–38 219, Dec 2019.

[5] Y. Ding, X. Liu, Z. rong Zheng, and P. fu Gu, "Freeform led lens for uniform illumination," *Opt. Express*, vol. 16, no. 17, pp. 12 958–12 966, Aug 2008.

[6] F. Fang, X. Zhang, A. Weckenmann, G. Zhang, and C. Evans, "Manufacturing and measurement of freeform optics," *CIRP Annals*, vol. 62, no. 2, pp. 823–846, 2013.

[7] C. Peixoto, P. T. Valentim, P. C. Sousa, D. Dias, C. Araújo, D. Pereira, C. F. Machado, A. J. Pontes, H. Santos, and S. Cruz, "Injection molding of high-precision optical lenses: A review," *Precision Engineering*, vol. 76, pp. 29–51, 2022.

[8] J. Rejc, J. Cinkelj, and M. Munih, "Dimensional measurements of a gray-iron object using a robot and a laser displacement sensor," *Robotics and Computer-Integrated Manufacturing*, vol. 25, no. 2, pp. 155–167, 2009.

[9] M. Grasso and B. Colosimo, "Process defects and in situ monitoring methods in metal powder bed fusion: a review," *Measurement Science and Technology*, vol. 28, p. 044005, 2017.

[10] P. Chiariotti, M. Fitti, P. Castellini, S. Zitti, M. Zannini, and N. Paone, "Smart quality control station for non-contact measurement of cylindrical parts based on a confocal chromatic sensor," *IEEE Instrumentation & Measurement Magazine*, vol. 21, no. 6, pp. 22–28, 2018.

[11] E. Csencsics, M. Thier, S. Ito, and G. Schitter, "Supplemental peak filters for advanced disturbance rejection on a high precision endeffector for robot-based inline metrology," *IEEE/ASME Transactions on Mechatronics*, vol. 27, no. 4, pp. 2258–2266, 2022.

[12] R. Henselmans, L. Cacace, G. Kramer, P. Rosielle, and M. Steinbuch, "The nanomefos non-contact measurement machine for freeform optics," *Precision Engineering*, vol. 35, no. 4, pp. 607–624, 2011.

[13] C. Haider, M. E. Fuerst, M. Laimer, E. Csencsics, and G. Schitter, "Range-extended confocal chromatic sensor system for double-sided measurement of optical components with high lateral resolution," *IEEE Transactions on Instrumentation and Measurement*, vol. 71, pp. 1–8, 2022.

[14] D. Wertjanz, E. Csencsics, T. Kern, and G. Schitter, "Bringing the lab to the fab: Robot-based inline measurement system for precise 3-d surface inspection in vibrational environments," *IEEE Transactions on Industrial Electronics*, vol. 69, no. 10, pp. 10 666–10 673, 2022.

[15] D. Wertjanz, T. Kern, A. Pechhacker, E. Csencsics, and G. Schitter, "Robotic precision 3d measurements in vibration-prone environments enabled by active six dof sample-tracking," in *2022 IEEE/ASME International Conference on Advanced Intelligent Mechatronics (AIM)*, 2022, pp. 1441–1446.

[16] M. E. Fuerst, E. Csencsics, C. Haider, and G. Schitter, "Confocal chromatic sensor with an actively tilted lens for 3d measurement," *J. Opt. Soc. Am. A*, vol. 37, no. 9, pp. B46–B52, Sep 2020.

[17] L. Guo, D. Martin, and D. Brunnett, "Dual-stage actuator servo control for high density disk drives," in *1999 IEEE/ASME International Conference on Advanced Intelligent Mechatronics (Cat. No.99TH8399)*, 1999, pp. 132–137.

Post-print version of the article: D. Wertjanz, T. Kern, E. Csencsics, and G. Schitter, "Robot-based measurement system for double-sided inspection of optical components," *2023 IEEE International Instrumentation and Measurement Technology Conference (I2MTC)*, Kuala Lumpur, Malaysia, 2023. DOI: 10.1109/I2MTC53148.2023.10175937